2017

Cross-Sectional Transport Imaging in a Multijunction Solar Cell

Haegel, Nancy M.

Cross-Sectional Transport Imaging in a Multijunction Solar Cell

Nancy M. Haegel, Chi-Wen Ke, Hesham Taha, Harvey Guthrey, Christopher M. Fetzer, and Richard R. King

***Abstract*—We combine a highly localized electron-beam point source excitation to generate excess free carriers with the spatial resolution of optical near-field imaging to map recombination in a cross-sectioned multijunction ($Ga_{0.5}In_{0.5}P/GaIn_{0.01}As/Ge$) solar cell. By mapping the spatial variations in emission of light for fixed generation (as opposed to traditional cathodoluminescence (CL), which maps integrated emission as a function of position of generation), it is possible to directly monitor the motion of carriers and photons. We observe carrier diffusion throughout the full width of the middle (GaInAs) cell, as well as luminescent coupling from point source excitation in the top cell GaInP to the middle cell. Supporting CL and near-field photoluminescence (PL) measurements demonstrate the excitation-dependent Fermi level splitting effects that influence cross-sectioned spectroscopy results, as well as transport limitations on the spatial resolution of conventional cross-sectional far-field measurements.**

***Index Terms*—Cathodoluminescence (CL), diffusion, luminescent coupling, multijunction solar cell, transport imaging.**

I. Introduction

TRANSPORT of photogenerated carriers is a critical component of solar cell operation. Although the cumulative response to broadband emission uniformly distributed across a full device results in an overall efficiency, the ability to directly observe energy transport associated with internal motion of either charge carriers or photons at any given point in the structure can provide valuable insight into key mechanisms determining that efficiency. We describe here the first transport imaging using combined electron beam excitation and near-field scanning optical microscopy (NSOM) to map photon emission associated with carrier recombination and optical transport in response to point source excitation in a cross-sectioned multijunction ($Ga_{0.5}In_{0.5}P$/ $GaIn_{0.01}As$/ Ge) solar cell. Transport imaging in photovoltaic devices is most interesting in cross section since one can image transport in the relevant direction for device operation. These results were presented for the first time at the 2015 Photovoltaics Specialty Conference [1]. This paper has been enhanced with additional spectroscopy results and expanded evaluation and explanation of the transport images.

It is critical to understand the difference between transport imaging, as will be presented here in Figs. 6 and 7, as well as traditional scanning photoluminescence (PL) and cathodoluminescence (CL). In both CL and PL imaging, the point of excitation is scanned; resultant luminescence is collected and mapped to the point of origin. This luminescence may be spectrally resolved, but it is not spatially resolved—one assumes that all luminescence arises from the point of excitation. This assumption is required because the optical collection area is generally large compared to the area of excitation.

In transport imaging, we maintain the spatial distribution of the luminescence resulting from excitation at a fixed point. This allows direct visualization of carrier diffusion, drift, or luminescent coupling, i.e., any process that results in photon emission at a location is spatially removed from the point of excitation. Since it gives direct access to the transport of minority carriers in doped semiconductor materials, transport imaging with far-field collection has most recently been used to measure minority carrier diffusion lengths and associated *minority* carrier mobilities in GaInP as a function of both doping and temperature [2], [3]. This was accomplished by studying specially designed double heterostructures of GaInP, which is the top cell material in the highest efficiency multijunction devices, and imaging resulting transport in the plane. Direct measurement of minority carrier mobility, which is difficult to achieve in other ways, has provided new insight into the physics of minority carrier mobility and, in particular, in the variations from the behavior of electrons in a majority carrier role. In this work, we apply this technique for the first time to image transport in the perpendicular direction in an actual multijunction device, imaging carrier, and photon motion in the direction of transport in an operating device.

Efforts to increase the efficiency in multijunction solar cells toward the 50% milestone include increasing the number of junctions to provide more efficient absorption, developing new materials systems, and applying increasingly sophisticated models to optimize luminescent coupling [4]–[6]. High-resolution spectroscopy techniques are required to study these multilayer systems. While a majority of CL work on multijunction cells has focused on defect mapping [7], [8] or studies of radiation damage [9], [10], transport imaging has the potential to provide important corollary information and directly evaluate materials properties, image interface, and junction recombination behavior and observe and quantify luminescent coupling.

Manuscript received May 11, 2016; revised September 24, 2016; accepted October 17, 2016. Date of publication December 1, 2016; date of current version December 20, 2016. This work was supported at the Naval Postgraduate School in part by the National Science Foundation under Grant DMR-0804527 and in part by the Laboratory and Directed Research and Development program at the National Renewable Energy Laboratory. The work of N. M. Haegel was supported by the Fulbright Senior Scholar Award.

N. M. Haegel and H. Guthrey are with the National Renewable Energy Laboratory, Golden, CO 80401 USA (e-mail: nancy.haegel@nrel.gov; harvey.guthrey@nrel.gov).

C.-W. Ke is with the Naval Postgraduate School, Monterey, CA 93943 USA (e-mail: chiwenke@hotmail.com).

H. Taha is with Nanonics Imaging Ltd., Jerusalem 9777518, Israel (e-mail: hesham@nanonics.co.il).

C. M. Fetzer and R. R. King are with the Boeing Spectrolab, Sylmar, CA 91342 USA (e-mail: christopher.m.fetzer@boeing.com; richard.r.king@asu.edu).

Color versions of one or more of the figures in this paper are available online at http://ieeexplore.ieee.org.

Digital Object Identifier 10.1109/JPHOTOV.2016.2623088

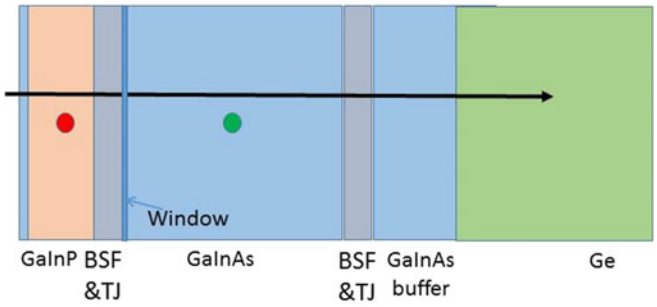

Fig. 1. Cross-sectional schematic of the structure. BSF: back surface field; TJ: tunnel junction. Figure is not to scale. For a more detailed schematic of a state-of-the-art multijunction cell, see [7].

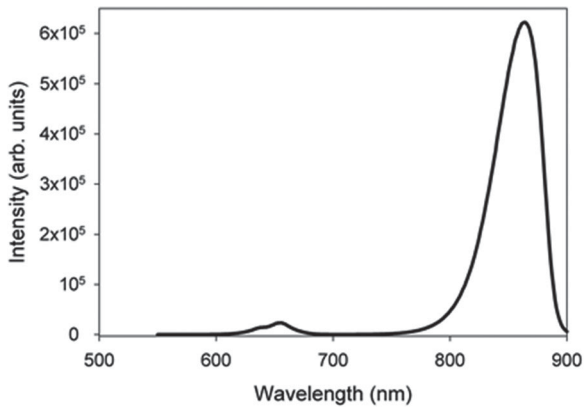

Fig. 2. CL intensity as a function of wavelength resulting from excitation at a point in the center of the top (GaInP) cell.

II. Experimental Results: Cathodoluminescence and Near-Field Photoluminescence

The sample is a triple junction GaInP/GaInAs/Ge device grown by metal–organic chemical vapor deposition. It was cleaved in air and mounted vertically to expose a cross-sectional surface.

Since transport imaging depends on emitted light, we initially perform CL spectroscopy to identify the origin and relative intensities of the luminescence emitted as a function of excitation position; this is an important step prior to transport imaging work in a complex multilayer structure. Fig. 1 shows a schematic cross section of the sample. We will refer to Fig. 1 repeatedly throughout the paper to describe multiple experiments.

Standard CL spectra were collected with a parabolic mirror, dispersed with a $1/4$ m path length monochromator and detected with a cooled GaAs PMT. We begin with point source excitation in the GaInP and GaInAs layers. An e-beam excitation energy of 5 kV was used, to limit the generation volume to within the layers of interest. To confirm this, the CL carrier generation volume was determined by Monte Carlo electron energy loss simulations using CASINO software [11]. The lateral dimension of carriers generated by the electron beam, defined by the region where 99% of the incident electron beam energy was lost, was found to be 230 nm at 5 keV.

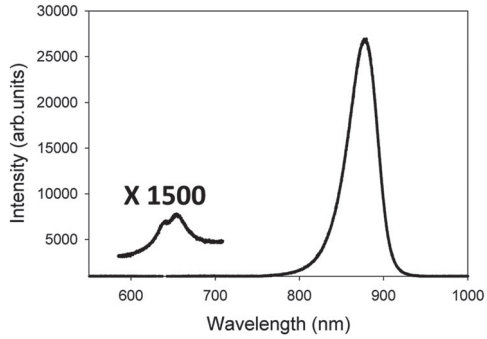

Fig. 3. CL intensity as a function of wavelength resulting from excitation at a point in the center of the middle (GaInAs) cell.

Fig. 2 shows a room temperature CL spectrum obtained for a point of excitation in the center of GaInP cell (e.g., the red point in Fig. 1). Layer thicknesses were determined using cross-sectional energy dispersive X-ray spectroscopy by mapping composition variations across the structure. This then allowed placement of the beam at a given position relative to the layers of interest. Note that excitation in the $\sim$1 μm thick GaInP layer produces luminescence both from that layer and from the GaInAs layer due to luminescent coupling. The intensity of the 880 nm peak measured from the GaInAs layer is larger only due to the combined effects of the responsivity of the GaAs PMT detector and the 1 μm blaze of the monochromator grating. No attempt should be made here to draw conclusions from the absolute intensities. Since the data are taken at room temperature, the line widths are thermally determined and fully resolved with a system resolution of 3 nm.

Fig. 3 shows a room temperature CL spectrum obtained for a point of excitation in the center of the $\sim$4 μm thick GaInAs cell (e.g., the green point in Fig. 1). Again, the generation volume associated with the low excitation energy means that direct generation of carriers occurs only in the GaInAs layer. However, we observe a weak, but measureable, luminescence signal at $\sim$660 nm, which is indicative of luminescence from the GaInP material. This is surprising, given that the generation volume is restricted to the GaInAs material, as described above, and will be discussed further below.

The luminescence from a single fixed point excitation in a multilayer structure will be a combination of response at the point of excitation, as well as emission associated with carrier diffusion, luminescent coupling, and any other coupling mechanisms in the device. This is especially relevant in high quality materials where the diffusion lengths can greatly exceed the layer dimensions and is evident in Figs. 2 and 3 with multiple wavelength emissions for a point source excitation in a single material. To further explore these coupling mechanisms, therefore, we performed CL line scans (see the black line in Fig. 1), using the monochromator to allow for selective monitoring of either 880 (GaInAs) or 660 nm CL (GaInP) as a function of position. This allows one to see the variation in intensity of a particular luminescence emission as a function of excitation position. Results are presented in Fig. 4 with the maximum intensity in both cases normalized to one.

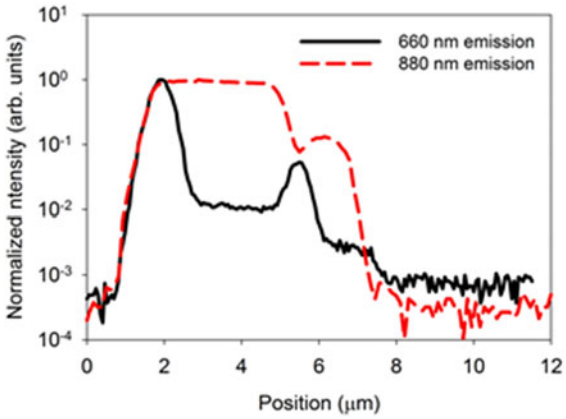

Fig. 4. CL intensity as a function of position for scan direction, as indicated by the black line in Fig. 1. The GaInAs cell in this device is ∼4 μm thick and extends from $x = 1.5$ to 5.5 μm in this image, followed by a buffer region, as shown in Fig. 1. The GaInP cell is on the left in this image, which is also shown in Fig. 1.

The 660 nm luminescence increases, as expected, as the beam enters the GaInP cell, decreases (but does not reach the background level) in the GaInAs middle cell, and then increases again in the BSF and TJ regions, which contain GaInP [7], before dropping to the background level in the Ge. An 880 nm signal is produced by excitation both in the GaInP as well as the GaInAs. The region from ∼5.5 to 7.5 μm is the GaInAs buffer layer. The absolute value of x is arbitrary, since it is determined simply by the beam starting location.

There are two important results to note in Fig. 4. First, the spatial variation of the integrated 880 nm emission shows the effect of luminescent coupling, with excitation in the GaInP layer producing coupled 660 and 880 nm emission. Second, excitation in the GaInAs middle layer clearly produces a much less intense but still measurably above-background luminescent signal at 660 nm, confirming the observation from point source CL in Fig. 3. This is the first known observation of this effect in cross-sectional CL. The large difference in intensity between the GaInAs emission and the higher energy 660 nm light means that this effect would not be easily recognized if data were presented on a linear scale. This 660 nm emission when exciting in the lower bandgap GaInP has been observed under varying excitation energies (5 to 15 keV) and probe currents (1×10^{-11} A to 6×10^{-10} A).

Consider this last observation further. Since the photon energy for 660 nm emission (1.88 eV) is larger than the 1.42 eV GaInAs bandgap, and we expect rapid thermalization of the carriers generated by the electron beam in GaInAs, this 660 nm emission cannot be the result of luminescent coupling or carrier diffusion. As mentioned earlier, the low excitation energy rules out the effect of extended generation volume directly exciting the GaInP material. The constant intensity of 660 nm emission for excitation throughout the layer also supports a different mechanism driving the red emission.

We hypothesize that point source excitation in the middle cell can cause an internal voltage and resultant splitting of quasi-Fermi levels in the GaInP window and back-surface field (BSF) layers of the middle cell. Since the observed luminescence is at 660 nm, it seems clear that its origin is one or more of the GaInP layers in the stack. The tunnel junction is very effective at inducing electron–hole recombination, and therefore, minority carriers are not able to diffuse through the tunnel junction to the GaInP top cell. Since there is no forward voltage bias of the GaInP top cell during the measurement and no current flowing through the top cell, and since there is no direct excitation of electron–hole pairs in the GaInP top cell base when the electron beam is focused on the GaInAs middle cell, the source of the 660 nm luminescence is likely not the top cell base. On the other hand, since interface recombination velocity at the GaAs/GaInP interface can be very small, i.e., as low as 1.5 cm/s [12] or lower, it is likely that the quasi-Fermi level splitting due to electron beam excitation in the GaInAs base persists past the GaInAs/GaInP interface for both the window and BSF layers. This results in a nonzero p-n product in these GaInP barrier layers which should produce a low but nonzero rate of radiative recombination emitting light at 660 nm. Internal waveguiding of light in these multiple very thin layers may also enhance the intensity of this emission from a cross-sectional sample. Therefore, a reasonable hypothesis is that the observed 660 nm emission is due to radiative recombination of these excess carriers, but this would require further investigation to fully confirm. Ideally, a dual probe measurement could confirm the exact spatial origin of the 660 nm emission, but the intensity is too low to allow for significant collection through a near-field aperture.

Finally, we performed high-resolution cross-sectional near-field scanning PL, using a Nanonics Multiview 4000 atomic force microscope (AFM)/NSOM, to provide a high-resolution baseline luminescence image for interpreting the transport results. Two forms of imaging were performed: 1) far-field excitation (532 nm) through a 50x microscope objective, with near-field PL collection using an optical fiber probe with a 150 nm aperture, and 2) near-field excitation (532 nm) through a multimode fiber with a 150 nm aperture, with far-field collection through the same upright objective. An Si photodiode was used for detection. In the absence of significant carrier transport effects, these two experiments would be expected to produce a similar result, since one would detect only from the sampled near-field region. However, transport of carriers from the point of excitation will reduce the effective spatial resolution, especially for the measurements with far-field excitation, which creates a larger excited volume that can contribute to emission at a particular near-field detection location. The direct comparison of the two approaches, therefore, is of interest as we develop these cross-sectional near-field analytical techniques.

Fig. 5 shows a cross-sectional PL image (Case B—near-field excitation and far-field detection), as well as a comparison of PL intensity as a function of position for the two approaches, A and B. The PL signal is combined emission at 660 and 880 nm. One sees the significant difference in spatial resolution. Near-field excitation produces the higher resolution result, consistent with the diffusion behavior for the far-field excitation discussed above.

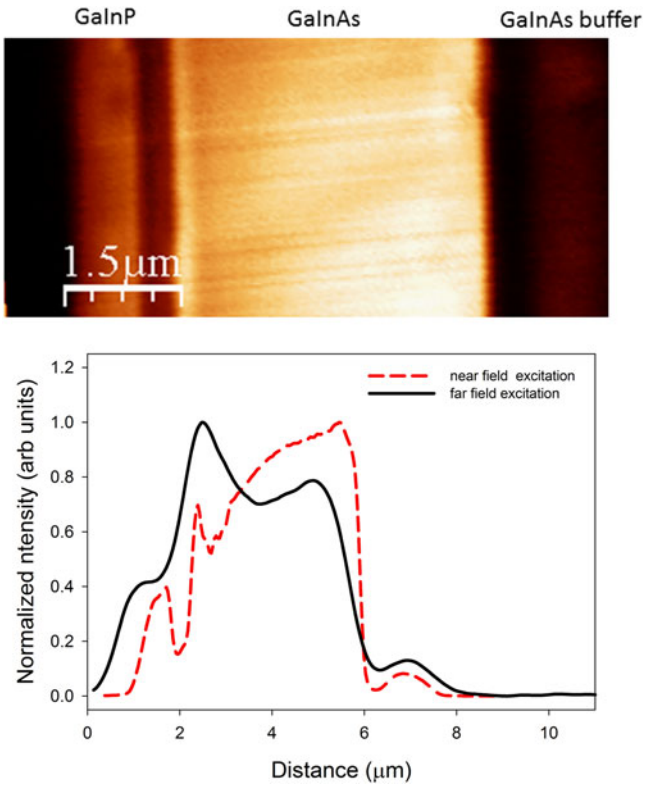

Fig. 5. Cross-sectional near-field PL image (top) and plot of normalized intensity (all wavelengths) as a function of position (bottom) comparing near-field excitation/far-field detection (red dashed) and far-field excitation/near-field detection (black solid).

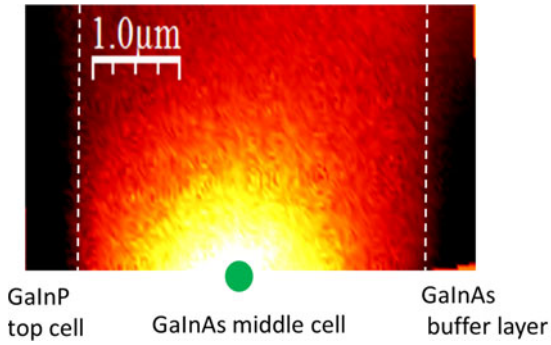

Fig. 6. Spatially resolved 880 nm luminescence in response to point source excitation in the middle cell. (Position of excitation indicated schematically by the green circle, as in Fig. 1). Intensity scale is white (high) to black (low). The white lines indicate interfaces defined by the tunnel junctions and back surface field.

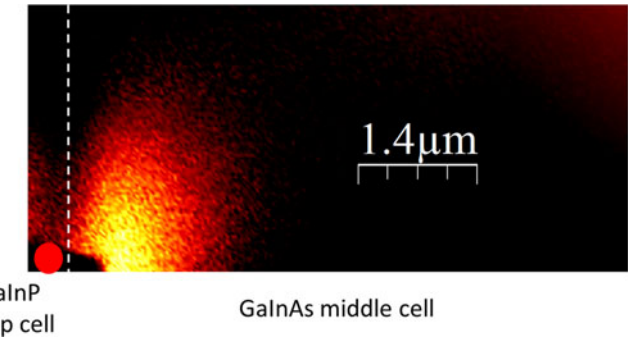

Fig. 7. Spatially resolved 880 nm luminescence in response to point source excitation in the top cell (position of excitation indicated schematically by the red circle, as in Fig. 1). Intensity scale is white (high) to black (low). The white line indicates the interface defined by the tunnel junction and back surface field.

III. Experimental Results: Transport Imaging

With an understanding of the spectroscopy for excitation in cross section, and with clear evidence of significant carrier diffusion, as shown in the comparison of the resolution of the near-field line scans in Fig. 5, we then performed the "dual probe" transport imaging measurements. The AFM/NSOM is mounted inside an FEI Inspect 50 scanning electron microscope. A detailed description of the integrated system for near-field transport imaging has been previously published [13], [14]. We excite with the electron beam at individual fixed points in the GaInAs (green circle) and the GaInP (red circle) layers (as indicated in Fig. 1). The device is open circuit.

For transport imaging, the SEM is operated with a fixed beam in "spot mode," while the spatial variation of the resulting luminescence is mapped by scanning the NSOM probe in a region *immediately adjacent to the excitation point*. The near-field luminescence was collected through a multimode fiber with a 200 nm aperture, scanning in steps of ~25 nm. Bandpass filters were used to select the 880 and 660 nm luminescence signals.

Fig. 6 shows the spatial variation of emission of 880 nm light resulting from electron-beam excitation at the green dot. As carriers diffuse, some fraction will recombine. We observe minority carrier diffusion throughout the full width of the GaInAs absorber, reflecting the large diffusion lengths in these high quality materials. The sharp cut-off in emission that occurs at the interfaces defined by the tunnel junction and the BSF suggests carrier diffusion as the dominant transport mechanism. An optical transport mechanism would be expected to include some transport of photons through the BSF/TJ to the GaInAs buffer layer beyond. This is not observed, even when the excitation point is moved very close to the interface. The nature of the luminescence distribution indicates a smooth diffusion profile and the absence of any significant localized recombination, either radiative or nonradiative. Values for the effective minority carrier diffusion length can be extracted if surface recombination velocity is accounted for. Modeling has been done to fit a variable value of the surface recombination velocity, but this analysis has yet to be done for the cleaved surface samples [15]. It is known that the minority carrier diffusion length in the bulk GaInAs material far exceeds the dimension of the middle cell [16], as seen in the image.

In Fig. 7, we again image luminescence at 880 nm this time resulting from excitation in the GaInP top cell (red dot). The luminescence measured in the adjacent GaAs cell is due to luminescent coupling, i.e., radiation emission in the GaInAs layer as a result of photons generated in the GaInP that propagate and are absorbed in the lower bandgap material. The spatial distribution provides a map of this convolution of emission, absorption,

carrier generation, and recombination. The ability to directly image this phenomenon could be valuable to confirm modeling and experimental efforts to maximize the device efficiency through optimization of this internal energy transport.

IV. Significance and Summary

We have demonstrated a new approach for directly imaging energy transport in a multijunction solar cell. We observe minority carrier diffusion throughout the full width of the middle cell and luminescent coupling from the top to middle cell. CL spectroscopy and near-field PL measurements in cross section also demonstrate the role that energy transport can play in the characterization of these structures. Transport imaging, therefore, has the potential to provide added insight into device behavior and support further optimization of these increasingly complex, high-efficiency devices.

Acknowledgment

N. M. Haegel would like to acknowledge the Fulbright Senior Scholar Award that provided the opportunity to collaborate with H. Taha at Nanonics Imaging Ltd.

References

[1] N. M. Haegel *et al.*, "Cross-sectional transport imaging in a multijunction solar cell," in *Proc. IEEE Photovolt. Spec. Conf.*, 2015, vol. 42, pp. 1–3.
[2] F. J. Schultes *et al.*, "Temperature dependence of diffusion length, lifetime and minority carrier electron mobility in GaInP," *Appl. Phys. Lett.*, vol. 103, pp. 242106-1–242106-4, 2013.
[3] N. M. Haegel *et al.*, "Doping dependence and anisotropy of minority electron mobility in molecular beam epitaxy-grown p type GaInP," *Appl. Phys. Lett.*, vol. 105, pp. 202116-1–202116-5, 2014.
[4] R. R. King *et al.*, "Solar generations over 40% efficiency," *Prog. Photvolt., Res. Appl.* vol. 20, pp. 801–815, 2012.
[5] D. J. Friedman, J. F. Geitz, and M. A. Steiner, "Effect of luminescent coupling on the optimal design of multijunction solar cells," *J. Photovolt.*, vol. 4, pp. 986–990, 2014.
[6] F. Dimroth *et al.*, "Four-junction wafer-bonded concentrator solar cells," *J. Photovolt.*, vol. 6, pp. 343–349, 2016.
[7] C. M. Fetzer *et al.*, "High-efficiency metamorphic GaInP/GaInAs/Ge solar cells grown by MOVPE," *J. Crystal Growth*, vol. 261, pp. 341–348, 2004.
[8] M. Stan *et al.*, "Very high efficiency triple junction solar cells grown by MOVPE," *J. Crystal Growth*, vol. 310, pp. 5214–5208, 2008.
[9] S. I. Maximenko, S. R. Messenger, C. D. Cress, J. A. Freitas, Jr., and R. J. Walters, "Application of CL/EBIC-SEM techniques for characterization of radiation effects in multijunction solar cells," *IEEE Trans. Nuclear Sci.*, vol. 57, no. 6, pp. 3095–3100, Dec. 2010.
[10] S. I. Maximenko *et al.*, "Characterization of high fluence irradiations on advanced triple junction solar cells," in *Proc. IEEE Photovolt. Spec. Conf.*, 2013, pp. 2979–2800.
[11] H. Demers, N. Poirier-Demers, M. R. Phillips, N. de Jonge, and D. Drouin, "Three-dimensional electron energy deposition modeling of cathodoluminescence emission near threading dislocations in GaN and electron-beam lithography exposure parameters for a PMMA resist," *Microsc. Microanal.*, vol. 18, pp. 1220–1228, 2012.
[12] J. M. Olson, R. K. Ahrenkiel, D. J. Dunlavy, B. Keyes, and A. E. Kibbler, "Ultralow recombination velocity at Ga0.5In0.5P/GaAs heterointerfaces," *Appl. Phys. Lett.*, vol. 55, pp. 1208–1210, 1989.
[13] N. M. Haegel, "Integrating electron and near-field optics: dual vision for the nanoworld," *Nanophotonics*, vol. 3, pp. 75–89, 2014.
[14] N. M. Haegel, D. J. Chisholm, and R. A. Cole, "Imaging transport in nanowires using near-field detection of light," *J. Crystal Growth*, vol. 352, pp. 218–223, 2012.
[15] K. E. Blaine, D. J. Phillips, C. L. Frenzen, C. Scandrett, and N. M. Haegel, "Three-dimensional transport imaging for the spatially resolved determination of carrier diffusion length in bulk materials," *Rev. Sci. Instrum.*, vol. 83, 2012, Art. no. 043701.
[16] N. M. Haegel *et al.*, "Direct imaging of anisotropic minority carrier diffusion in ordered InGaP," *J. Appl. Phys.*, vol. 105, 2009, Art. no. 023711.

Authors' photographs and biographies not available at the time of publication.